Materials Advances

PAPER

Check for updates

HCl-assisted fabrication of metal–organic framework UiO-66(Zr) for affordable gas capture

Zineb Ouzrour,[a] El Mehdi Moumen,[b] Ran Eitan Abutbul, [iD][c] Daniel Lee, [iD][c] Marta Falkowska,[c] Tausif Altamash, [iD][a] Samir El Hankari [iD][b] and Johan Jacquemin [iD] *[a]

The use of HCl as a modulator in synthesizing ubiquitous metal–organic framework UiO-66(Zr) from $ZrOCl_2 \cdot 8H_2O$ yields a CO_2 adsorption capacity comparable to that observed using the benchmark $ZrCl_4$ precursor. Both materials possess similar particle size, shape, and structural properties, as well as CO_2 capture capability when the material activation temperature is optimized. The findings of this work highlight the possibility of preparing UiO-66 MOF under more affordable conditions by using the $ZrOCl_2 \cdot 8H_2O$ precursor and the HCl modulator than the current benchmark without affecting its properties.

Metal–organic frameworks (MOFs) are crystalline porous materials composed of metal clusters and organic linkers. Their high surface areas, tunable pore structures, and modular design make them highly attractive for applications in drug delivery,[1] batteries,[2,3] and particularly gas capture and separation.[4,5] Compared with traditional porous materials such as zeolites, activated carbons or biomass-based sorbents,[6–8] MOFs offer high structural flexibility and chemical tunability, which enable tailored host–guest interactions.[9,10]

Over the past few years, significant progress has been made in the field of MOFs for gas capture, especially in CO_2 adsorption, CH_4 storage, H_2 purification, and selective separation of industrially important gases.[11–13] Research groups such as those of Yaghi, Gao and Amenitsch are among many that have focused on strategies to modify MOF properties.[14–17] Strategies such as linker functionalization, integration of open metal sites, or incorporation of MOFs into membranes or composites significantly modify the pore diffusivity and enhance gas uptake and selectivity.[18–21] In particular, defect engineering has recently emerged as a potential strategy to adjust MOF properties.[22] By introducing missing linkers or clusters, researchers have been able to increase porosity and active sites, enhancing CO_2 uptake capacity and CO_2 affinity.[22–26]

Despite these improvements, challenges remain for scaling MOFs toward industrial gas capture.[27] A central barrier is the high cost of synthesis, since many MOFs depend on expensive metal precursors, costly organic linkers, and modulators that complicate the process (cost(HSKUT-1) = cost(UiO-66) = cost(MOF-5) = 50\$ g^{-1}).[28–32]

Zirconium-based metal–organic frameworks are one of the most investigated families of MOFs owing to their thermal, chemical, and mechanical stability, the strong Zr–O bonds and the high degree of connectivity of their clusters. The best known is UiO-66.[33,34]

UiO-66, developed at the University of Oslo, has attracted tremendous attention over recent years.[35]

UiO-66 is built up of centric octahedral cages, and each of them is linked with eight corner tetrahedral cages through triangular windows.[36,37] This MOF exhibits a high surface area of 600 to 1800 m^2 g^{-1} and high stability, particularly hydrothermal stability up to 500 °C, which surpass those of most other reported MOFs.[38–41]

UiO-66(Zr) is commonly synthesized by mixing a terephthalic acid (BDC) ligand with a zirconium (Zr) source precursor such as $[Zr(NO_3)_4 \cdot 5H_2O]$, $[ZrO(NO_3)_2 \cdot 4H_2O]$, $[Zr(SO_4)_4]$, or $[ZrOCl_2 \cdot 8H_2O]$.[42,43] Nevertheless, $ZrCl_4$ represents the benchmark Zr precursor, which reliably yields highly crystalline and stable materials.[44] However, $ZrCl_4$ has significant challenges due to its cost and instability in pure water, leading to a violent exothermic hydrolysis reaction. Additionally, its exposure to humid air leads to the formation of a mixture of $ZrCl_4$ and $ZrOCl_2 \cdot 8H_2O$, causing some difficulties in the handling process of this precursor, which requires an inert atmosphere and thus complicates the production of materials with reproducible resulting properties.[45] Therefore, large-scale preparation of UiO-66 requires more affordable alternatives. One such candidate is $ZrOCl_2 \cdot 8H_2O$, which is cheaper and widely available, yet

[a] *Materials Science and Nano-engineering (MSN) Department, Mohammed VI Polytechnic University (UM6P), Lot 660-Hay Moulay Rachid, 43150, Benguerir, Morocco. E-mail: Johan.jacquemin@um6p.ma*

[b] *Chemical and Biochemical Sciences (CBS) Department, Mohammed VI Polytechnic University (UM6P), Lot 660-Hay Moulay Rachid, 43150, Benguerir, Morocco*

[c] *Department of Chemical Engineering, University of Manchester (UoM), Oxford Rd, Manchester, M13 9PL, UK*
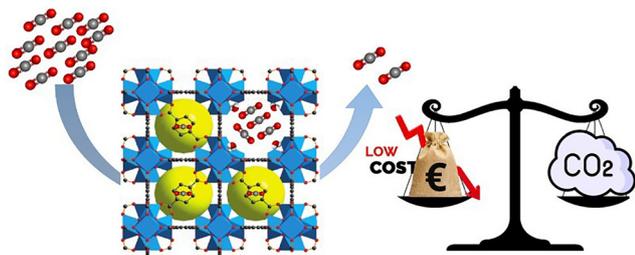
Fig. 1 Schematic of the concept applied during this study: enhancing CO_2 adsorption through defects and balancing cost and capacity compared to a conventional UiO-66 benchmark.

Fig. 2 SEM images of the samples: (a) and (b) 1-U, (c) and (d) 2-U, and (e) and (f) 2-U-HCl.

not much explored as a UiO-66 precursor. Its combination with simple modulators, such as HCl, offers the potential to reduce costs without compromising performance.[46]

Thus, as shown in Fig. 1, this work aimed to prepare defective UiO-66(Zr) from $ZrOCl_2 \cdot 8H_2O$ with a morphology similar to that of UiO-66(Zr) synthesized using expensive $ZrCl_4$, by pre-adding HCl to $ZrOCl_2 \cdot 8H_2O$ to avoid the formation of a hydrated UiO-66 gel with a low number of active sites. Thus, the objective is to increase the defects and active sites within UiO-66 synthesized from $ZrOCl_2 \cdot 8H_2O$ to increase its capability for CO_2 adsorption.

During this work, three different UiO-66 samples were synthesized by using (i) $ZrCl_4$ by conventional means[47] in the presence of HCl (1-U), (ii) $ZrOCl_2 \cdot 8H_2O$ without HCl (2-U),[48] and (iii) $ZrOCl_2 \cdot 8H_2O$ with HCl as a modulator, which pre-reacts with $ZrOCl_2 \cdot 8H_2O$ for 30 minutes, subsequently yielding a new MOF, named herein 2-U-HCl (full synthesis details are given in the SI). While UiO-66 synthesized from $ZrCl_4$ (1-U) using dimethylformamide (DMF) as solvent yielded a white powder, 2-U and 2-U-HCl formed a yellow gel and a white powder, respectively (see the SI).

Scanning electron microscopy (SEM) was used to investigate the surface morphology and particle sizes of the materials. As shown in Fig. 2 and Fig. S3–S5 of the SI, 1-U is defined by small crystalline particles of 10 nm in size. The use of the strong acidic modulator HCl facilitated the particle nucleation and terminated the growth of 1-U. This contrasts with 2-U, where the absence of the acidic modulator resulted in larger cumulative agglomerated particles of approximately 3 μm. Upon introducing the HCl modulator for 2-U-HCl, a noticeable transformation in particle angularity and size occurs. These particles exhibit clarity and relative reduction in size, similar to those observed for conventionally synthesized 1-U.

The powder X-ray diffraction (PXRD) patterns of all samples, depicted in Fig. 3 and Fig. S1 of the SI, reveal the presence of four distinct characteristic diffraction peaks situated at 2θ = 7.5°, 8.6°, 12.1°, and 14.7°, corresponding to reflections from the (111), (200), (220), and (311) crystallographic planes, respectively. Notably, the PXRD pattern of the obtained 1-U product shows a narrow (111) peak, with large intensity. This distinct peak profile signifies the attainment of a highly crystalline structure for 1-U, consistent with expectations.[24,28] In contrast, the PXRD pattern of 2-U presents weak and broad peaks that
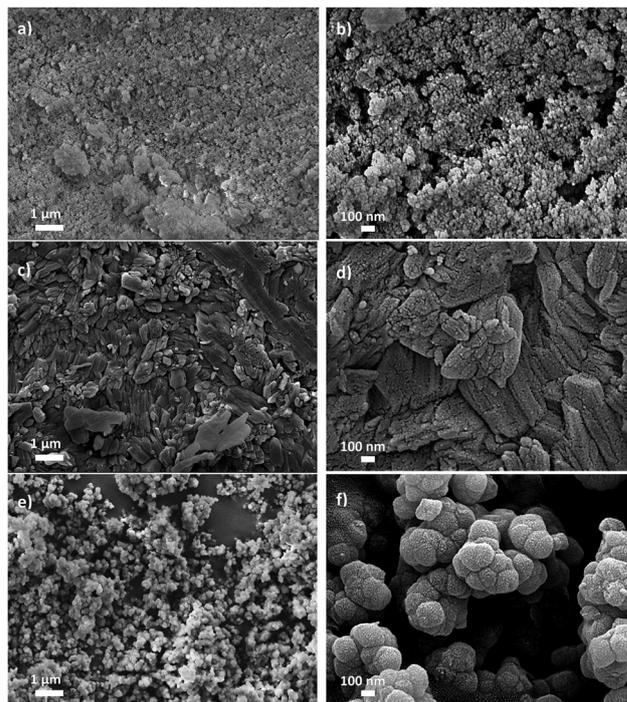
are nevertheless characteristic of UiO-66. This implies that 2-U has a lower degree of crystallinity, likely owing to numerous structural defects. This outcome can be attributed to the high water content present within the structure. This water presence hinders the deprotonation process of the ligand and reduces the number of available binding sites within the cluster.[49] Interestingly, the PXRD pattern of 2-U-HCl is very similar to that of 1-U, highlighting much increased crystallinity compared
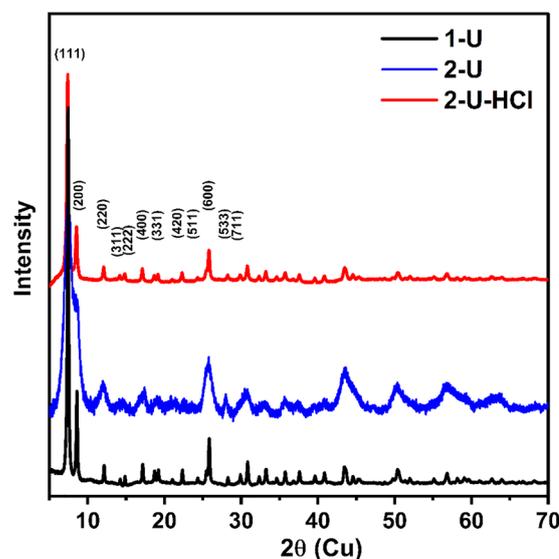

Fig. 3 XRD patterns of 1-U (bottom, black), 2-U (middle, blue), and 2-U-HCl (top, red).

to 2-U. This suggests that the modulator plays a role in minimizing the impact of water on the crystallinity of the MOF. These findings correspond well with the SEM results.[50]

To quantify the impact of the modulator on the defect density of synthesized samples, thermogravimetric analysis (TGA) was performed under atmospheric conditions, with the results shown in Fig. 4. This followed Lillerud's protocol[51] (see Fig. S2) which is based on two major assumptions: (i) the samples are of pure phase UiO-66 and (ii) the TGA product at 600 °C is a pure ZrO_2.[52] With these assumptions, the TGA curves for UiO-66 can be divided into three stages from room temperature to 100 °C, where solvents and adsorbed gases are removed; from 100 to 350 °C, involving the loss of solvents and the modulator; and from 350 to 600 °C, where organic linkers (BDC) are lost, leading to the formation of zirconium oxide (ZrO_2). The weight of ideal UiO-66 at 350 °C is 220.2%, which corresponds to the chemical formula $Zr_6O_6(BDC)_6$.[23] In contrast, defective UiO-66 has a weight below 220.2%, indicating a deficiency of BDC linkers. This defective form is represented by the formula $Zr_6O_{6+x}(BDC)_{6-x}$, where (x) denotes the number of missing linkers, calculated using specific equations reported in the SI. In our case, the experimental weight % determined using the TGA trace at 350 °C for 1-U, 2-U-HCl, and 2-U was 182%, 173%, and 161%, respectively. These results are lower than the expected weight (220% of ZrO_2), indicating that their structures have abundant linker defects. The number of these defects increases in the following order: 1-U < 2-U-HCl < 2-U. Consequently, the average missing-linker numbers were evaluated by considering an ideal number of ligands per cluster in a perfect UiO-66 structure, which equals 6. The calculated average missing-linker numbers for 1-U, 2-U-HCl, and 2-U were found to be 1.85, 2.30, and 2.87, respectively.

In light of the TGA, the surface analysis was performed to understand the morphology of the surface. The N_2 adsorption–desorption isotherm of 2-U shows a type H2 hysteresis loop,
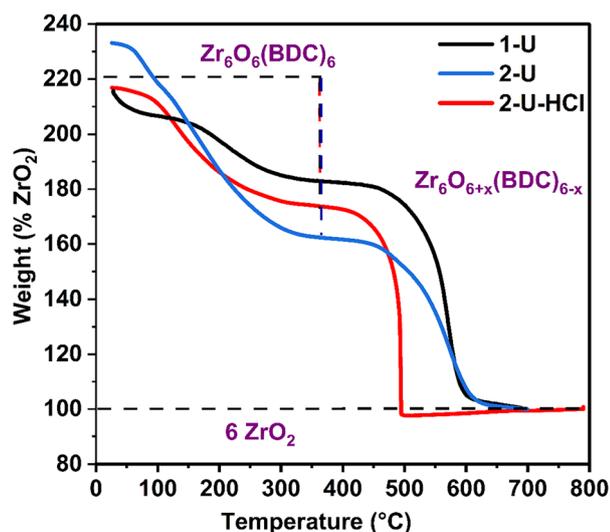
indicating disordered mesoporous structures with narrow necks and ink-bottle pores, as evidenced by pore blocking and cavitation effects. In contrast, 2-U-HCl and 1-U exhibit type I isotherms, characteristic of microporous structures, where adsorption primarily occurs at low relative pressures. These observations highlight the distinct textural properties of the materials. Also, different activation conditions, such as under vacuum (0.1 bar) and in air, temperatures (120 °C, 170 °C, and 300 °C) and times (4 h and 12 h), were applied to investigate their effect on the surface area of 1-U, 2-U and 2-U-HCl samples. These particular conditions were chosen because (i) 120 °C corresponds to the pretreatment used prior to CO_2 adsorption experiments, (ii) 170 °C corresponds to the pretreatment utilized before solid-state NMR measurements, and (iii) 300 °C was selected based on TGA measurements as the pure MOF is obtained at this temperature. As shown in Table S2 and Fig. S6 of the SI, the surface area of 2-U and 2-U-HCl after activation at 120 °C reaches a similar value below 600 m^2 g^{-1}, with a slightly higher surface area obtained for 1-U ($\sim$700 m^2 g^{-1}). Interestingly, the surface area for 2-U is in the range of 639–657 m^2 g^{-1} irrespective of the temperature or time of the sample pretreatment. For 2-U-HCl, the surface area is highly affected by the conditions of the activation procedure. Pretreatment at 120 °C for 4 h, 170 °C for 4 h and 300 °C for 4 h results in the 2-U-HCl sample with a surface area almost identical to the surface area determined for 2-U activated under the corresponding conditions. However, when a longer pretreatment (i.e. at 170 °C for 12 h or at 300 °C for 12 h) is performed, the surface area increases to 730–805 m^2 g^{-1}; however, this is still much lower than the surface area of 1326 m^2 g^{-1} reported for 1-U.[53] The XRD analysis (see Fig. S8 of the SI) of 2-U-HCl activated under different conditions (no activation and activation at 300 °C for 4 and 12 h) revealed the stability of its crystalline structure no matter the activation time and temperature applied. This shows that the solvent molecules physically occupied the active sites rather than being part of the main cluster, unlike in 2-U, where they are chemically bound to the structure.

^{1}H and ^{13}C solid-state magic angle spinning (MAS) NMR spectroscopies were utilized to study the atomic-scale structural differences between the investigated UiO-66(Zr) MOFs; this technique has been extensively employed for this purpose previously.[54,55] Each sample was analysed before and after activation at 170 °C overnight, as depicted in the SI.

Fig. 5 shows the corresponding {^{1}H–}^{13}C CPMAS spectra of the as-synthesized and activated MOFs. For 1-U, the main expected resonances from the BDC linker are present at $\delta(^{13}C)$ = 170, 137 and 129 ppm, but there are additional peaks at $\delta(^{13}C)$ = 162, 63, 34 and 29 ppm. The resonance at $\delta(^{13}C)$ = 170 ppm is associated with the chelating carboxylate group bound to Zr centres,[55] and the resonances at $\delta(^{13}C)$ = 137 and 129 are associated with para and meta carbons on the benzene ring in the BDC linker. DMF, the reaction solvent, has resonances at $\delta(^{13}C)$ = 162, 34, and 29 ppm. An ethoxy group appears with $\delta(^{13}C)$ = 63 and 20 ppm, which stems from the ethanol washing procedure. The 20 ppm peak slightly overlaps with a spinning side band that originates from the 137 ppm peak.
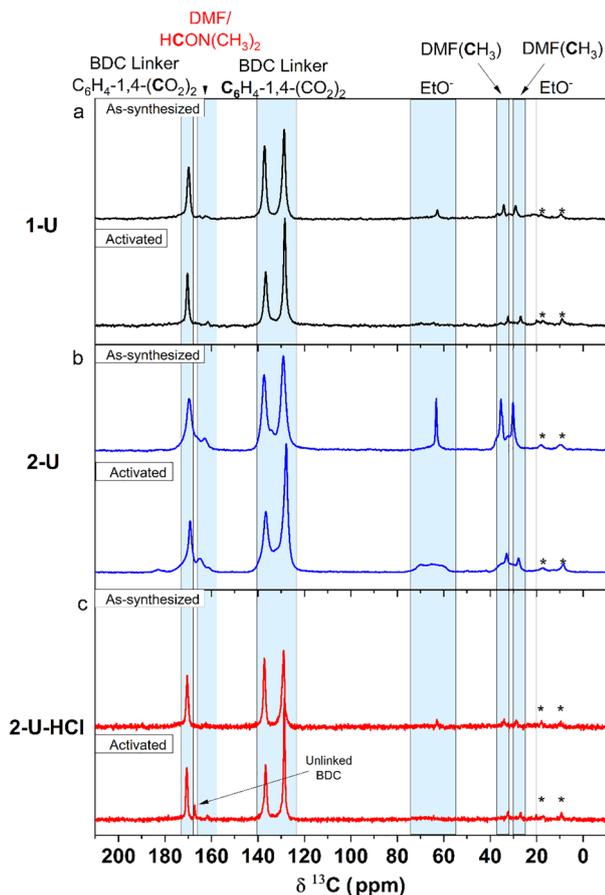

Fig. 4 TGA results normalized to weight percent of ZrO_2 for 1-U, 2-U, and 2-U-HCl samples.

Fig. 5 $\{^1H-\}^{13}C$ CPMAS NMR spectra of the as-synthesized and activated (170 °C overnight) (a) 1-U (black), (b) 2-U (blue) and (c) 2-U-HCl (red). Assignments are given with guides for the eye. * denotes spinning side bands.

Upon activation, the 63 ppm resonance disappears, indicating ethanol evaporation. The DMF peaks slightly shift, which suggests a transition to an energetically favourable position within the activated 1-U upon release of ethanol. BDC-linker peaks become narrower (*cf.* FWHM ~150 Hz to ~100 Hz), which indicates improved crystallinity after activation.

The as-sythesized 2-U contains significant amounts of solvents and by-products, including DMF and ethoxy groups, which are reduced, but not removed, after activation. It should be noted that for the ethoxy group, a resonance at around 20 ppm is expected for the methyl carbon. However, its absence likely indicates reduced reorientation dynamics of the methyl protons, owing to the pore confinement, which makes it more challenging to detect.[56] The frequencies associated with the ethoxy groups and DMF show both narrow and broad components. The narrow components are likely mobile or ordered species, while the broad ones will stem from structural disorder. An additional peak at $\delta(^{13}C) = 166$ ppm is present, which could be assigned to irregular BDC linker sites or rigid, bound DMF.[57–59] Both could be regarded as defect sites. Upon activation at elevated temperatures, the narrow components of the ethoxy and DMF resonances decrease substantially while the

broad components remain. This suggests that the mobile moieties are removed, and the more rigid molecules are not, even at elevated temperatures. The solvent molecules that remain, as the broad resonances suggest, are found in many different parts of UiO-66(Zr) as part of its structure. It should also be noted that BDC linker peaks in the activated 2-U are slightly narrower than those in as-synthesized 2-U (*cf.* FWHM ~250 Hz to ~200 Hz), but these are still relatively broad compared to 1-U.

The $\{^1H-\}^{13}C$ CPMAS NMR spectrum of the as-synthesized 2-U-HCl is similar to the corresponding spectrum of the as-synthesized 1-U (*cf.* Fig. 5a and c). Upon activation, a new resonance appears at $\delta(^{13}C) = 167$ ppm. This resonance is typical of the protonated acidic organic linker,[60] likely due to remaining HCl partially digesting the MOF at high temperatures.[60] Studies have confirmed that the presence of HCl can lead to the protonation of the carboxylic groups of the linker, leading to free acid linkers even in the absence of defects.

^1H MAS NMR spectra (shown in Fig. S7) support the conclusions drawn from the $\{^1H-\}^{13}C$ CPMAS NMR data. Initial inspection of the ^1H NMR spectra suggests that all samples can be divided into two main regions. The resonances at $\delta(^1H) = 0–5$ ppm are mainly associated with protons that reside on solvent molecules; DMF, ethoxy groups, and water are expected to exhibit ^1H resonances within this range. The resonances at $\delta(^1H) = 5–10$ ppm are associated with the BDC linkers and DMF. Comparing each pair of samples, the as-synthesized and activated, the region associated with solvents changes substantially upon activation compared to the region related to the BDC linkers. This result suggests that solvent molecules are evaporated from the investigated UiO-66(Zr) during the activation step. The ^1H resonances of the solvents can exhibit a wide range of chemical shifts as they can reside in many different conformations and orientations inside the UiO-66(Zr) pores.

Overall, the solid-state NMR results indicate a higher concentration of rigid, disordered defects that are not removed upon activation in the 2-U sample. The 2-U-HCl and 1-U MOFs behave similarly upon activation; solvents effectively leave the UiO-66(Zr) materials. However, a small number of defects remain in the 2-U-HCl sample, while the structure remains intact and crystalline. These defects may either aid or hinder the adsorption properties, depending on the host–guest interaction.

Based on the results of TGA, ^{13}C NMR spectroscopy, ^1H NMR spectroscopy, and XRD for 1-U, 2-U, and 2-U-HCl, it is evident that water plays a central role in determining the degree of hydroxylation and dihydroxylation in the UiO-66 frameworks. The synthesis of 1-U using $ZrCl_4$ as the Zr precursor, which introduces minimal water content, resulted in the formation of a stable MOF named 1-U and a highly crystalline framework with minimal structural defects, leading to the highest CO_2 uptake of 1.4 mmol g^{-1} at 1 bar due to an intact coordination environment and fully accessible adsorption sites.[61] In contrast, in 2-U, water molecules from the precursor became directly incorporated into the Zr clusters, leading to a higher degree of hydroxylation and dihydroxylation [hydroxyl(–OH)
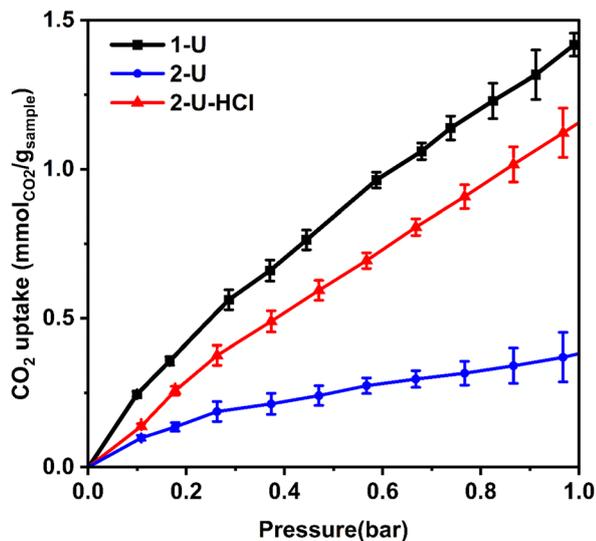
Fig. 6 CO_2 adsorption capacity for 1-U, 2-U, and 2-U-HCl at absolute CO_2 equilibrium pressures up to 1 bar and 298 K. Vertical error bars were calculated according to an error propagation method along with data reported in Tables S6 and S7 of the SI.

groups replaced some carboxylate linkers and two hydroxyl groups reacted to occupy the sites where linkers should have been]. This defect formation is evidenced by the significantly high number of defects and water present at lower temperatures in TGA, broadened carboxylate signals in the ^{13}C NMR spectrum, and Zr–OH peaks in the ^1H NMR spectrum. These weak interactions with CO_2 molecules result in a significant reduction in CO_2 uptake to only 0.42 mmol g^{-1} at 1 bar.[62] For the 2-U-HCl sample, HCl introduced during synthesis played a critical role in modifying the integration of excess water into the Zr clusters. The created acidic environment reduced the probability of water being directly integrated into the coordination cluster of zirconium, thus limiting the extent of hydroxylation and dihydroxylation.[63] Thereby, 2-U-HCl demonstrated a near CO_2 uptake of 1-U (1.22 mmol g^{-1} at 1 bar), showcasing the positive impact of HCl, as seen in Fig. 6.

A closer look at the isotherm fitting models (Fig. S10 and Table S3) provides further understanding about the nature of the adsorption sites of the samples, 1-U, 2-U, and 2-U-HCl, which exhibited good fitting with the Freundlich isotherm model, and adsorption occurring on heterogeneous surfaces in this study. Additionally, 2-U exhibited the highest Freundlich exponent ($n = 1.47$), followed by 2-U-HCl ($n = 1.45$) and 1-U ($n = 1.33$). The trends confirm that the degree of surface heterogeneity increases with the increasing number of structural defects, especially when these defects are not controlled. In contrast, 2-U-HCl, synthesized under acidic conditions, maintained moderate heterogeneity with improved adsorption affinity, signifying the role of HCl in modulating defect formation.[64] Moreover, the CO_2 cycling stability for 2-U-HCl was confirmed through multiple adsorption–desorption cycles (Fig. S11), displaying minimal capacity loss and excellent reversibility, which highlights its robustness and structural integrity. The nearly identical uptake values across five continuous cycles, ranging from 1.06 to 0.90 mmol g^{-1}, which demonstrate significant stability.[65] The adsorption and desorption cycles were performed at 120 °C and 25 °C, respectively. The consistent CO_2 release and uptake confirm that the process is fully reversible, and no chemisorption/hysteresis was observed throughout our experiments, as it was suggested by the fitted isotherm with Freundlich theory, with no pore collapse or degradation of the framework.[66,67]

To also further evaluate the impact of the activation conditions on the 2-U-HCl structure and its properties, CO_2 tests were conducted by varying the activation temperature and time set before starting CO_2 solubility measurements with this MOF. As shown in Fig. S12 of the SI, it appears that the CO_2 capacity of 2-U-HCl is strongly affected by the activation conditions applied. At 293 K and 1 bar, its CO_2 uptake increases from 0.57 mmol g^{-1}, for the non-activated sample, to 2.01 mmol g^{-1} when activating the sample at 300 °C for 12 h. This value is higher than the value obtained for 1-U (1.6 mmol g^{-1}) or others available in the literature, as reported in Tables S4 and S5 of the SI. These results align with the findings of Magnin's study,[68] which established that at low pressure of pure CO_2 and low loading of CO_2, both the CO_2 and H_2O molecules are adsorbed in the octahedral cages, but at a higher pressure of CO_2 and water loading, both molecules start to emerge in the tetrahedral ones, which causes an elevated competition between H_2O and CO_2, driving velocity and diffusion of CO_2. By reducing the number of solvent molecules in the structure *via* activation at 300 °C for 12 h, we reduce the water present in the active sites of the tetrahedral cages; therefore, the CO_2 uptake was maximized.

Our study further confirmed that HCl not only serves as a modulator but also reduces the interactions between the MOF and solvent molecules during the nucleation step, resulting in a structure with low water content upon activation.

In summary, the use of ZrOCl$_2$·8H$_2$O as a precursor, along with a modulator, for the synthesis of UiO-66(Zr) provides a MOF with CO_2 adsorption capabilities comparable to those observed for the equivalent MOF produced using the benchmark ZrCl$_4$. This has significant implications for an eco-friendly, cost-effective, and safer CO_2 capture and storage strategy using this particular MOF. We also showed that the applied activation conditions for this MOF are crucial for driving higher CO_2 uptake. More specifically, it was proven that 2-U-HCl can retain a high degree of crystallinity, comparable with the 1-U benchmark, over a wide range of activation conditions. It is expected that this finding could open new avenues for understanding the importance of defects in the adsorption of CO_2 and other gases. This provides the potential for fabricating various MOFs using different precursors. In our case, changes in the synthesis and activation processes affect many parameters, including the number of defects, crystallinity, thermal stability, and CO_2 adsorption capacity. This insight could lead to the development of more efficient and versatile MOFs for a wide range of applications in gas adsorption and separation. Additionally, understanding these

synthesis–activation–structure–property relationships can drive advancements in the design of next-generation MOFs with tailored functionalities from more and non-corrosive metal precursors.

Conflicts of interest

The authors declare that they have no conflicts of interest.

Data availability

The data supporting the findings of this study are available within the article and its supplementary information (SI). Supplementary information is available. See DOI: https://doi.org/10.1039/d5ma00461f.

Acknowledgements

Notes and references

1 Y. Si, H. Liu, M. Li, X. Jiang, H. Yu and D. Sun, *J. Colloid Interface Sci.*, 2023, **640**, 521–539.

2 X. Xu, Y. Xu, J. Zhang, Y. Zhong, Z. Li, H. Qiu, H. B. Wu, J. Wang, X. Wang, C. Gu and J. Tu, *Nano-Micro Lett.*, 2023, **15**, 1–15.

3 J. Hou, H. Zhang, J. Lu, X. Li, C. Zhao, H. Wang, A. W. Thornton and K. Konstas, *J. Membr. Sci.*, 2023, **674**, 121511.

4 M. Zhou and J. Wu, *npj Comput. Mater.*, 2022, **8**, 256.

5 Z. Liu, Y. Lu, C. Wang, Y. Zhang, X. Jin, J. Wu, Y. Wang, J. Zeng, Z. Yan, H. Sun and C. Wu, *Fuel*, 2023, **340**, 127476.

6 F. A. Abdul Kareem, A. M. Shariff, S. Ullah, N. Mellon and L. K. Keong, *Microporous Mesoporous Mater.*, 2018, **267**, 221–234.

7 A. Abdeljaoued, N. Querejeta, I. Durán, N. Álvarez-Gutiérrez, C. Pevida and M. H. Chahbani, *Energies*, 2018, **11**, 1–14.

8 H. Akaya, S. Lamnini, H. Sehaqui and J. Jacquemin, *ACS Appl. Mater. Interfaces*, 2025, **17**(11), 16380–16395.

9 V. F. Yusuf, N. I. Malek and S. K. Kailasa, *ACS Omega*, 2022, **7**, 44507–44531.

10 F. zohra Zeggai, Z. Ait-Touchente, K. Bachari and A. Elaissari, *Chem. Phys. Impact*, 2025, **10**, 100864.

11 R. Wei, T. Zhao, H. Xu and J. Gao, *Dalton Trans.*, 2025, **54**, 8385–8391.

12 L. Qiao, C. Lu, W. Fan, Z. Xue, X. Wang, Z. Kang and D. Sun, *Int. J. Hydrogen Energy*, 2024, **93**, 805–821.

13 C. Jiang, X. Wang, Y. Ouyang, K. Lu, W. Jiang, H. Xu, X. Wei, Z. Wang, F. Dai and D. Sun, *Nanoscale Adv.*, 2022, **4**, 2077–2089.

14 O. I.-F. Chen, C.-H. Liu, K. Wang, E. Borrego-Marin, H. Li, A. H. Alawadhi, J. A. R. Navarro and O. M. Yaghi, *J. Am. Chem. Soc.*, 2024, **146**, 2835–2844.

15 S. Klokic, B. Marmiroli, G. Birarda, F. Lackner, P. Holzer, B. Sartori, B. Abbasgholi-NA, S. Dal Zilio, R. Kargl, K. Stana Kleinschek, C. Stani, L. Vaccari and H. Amenitsch, *Nat. Commun.*, 2025, **16**, 7135.

16 M. Ding, R. W. Flaig, H.-L. Jiang and O. M. Yaghi, *Chem. Soc. Rev.*, 2019, **48**, 2783–2828.

17 R. Wei, T. Zhao, H. Xu and J. Gao, *Dalton Trans.*, 2025, **54**, 8385–8391.

18 J. Liu, C. Chen, K. Zhang and L. Zhang, *Chin. Chem. Lett.*, 2021, **32**, 649–659.

19 M. Alshurafa, A. B. Foster, S. Aloraini, M. Yu, B. Qiu, P. Gorgojo, M. P. Attfield and P. M. Budd, *J. Membr. Sci.*, 2025, **713**, 123388.

20 A. Torrisi, R. G. Bell and C. Mellot-Draznieks, *Cryst. Growth Des.*, 2010, **10**, 2839–2841.

21 M. Zhao, Y. Yang and X.-S. Gu, *Inorg. Chem. Commun.*, 2023, **152**, 110722.

22 J. Niu, H. Li, L. Tao, Q. Fan, W. Liu and M. C. Tan, *ACS Appl. Mater. Interfaces*, 2023, **15**, 31664–31674.

23 J. Yin, Z. Kang, Y. Fu, W. Cao, Y. Wang, H. Guan, Y. Yin, B. Chen, X. Yi, W. Chen, W. Shao, Y. Zhu, A. Zheng, Q. Wang and X. Kong, *Nat. Commun.*, 2022, **13**, 5112.

24 P. Chammingkwan, G. Y. Shangkum, L. T. T. Mai, P. Mohan, A. Thakur, T. Wada and T. Taniike, *RSC Adv.*, 2020, **10**, 28180–28185.

25 Y. Cao, X. Mi, X. Li and B. Wang, *Front. Chem.*, 2021, **9**, DOI: 10.3389/fchem.2021.673738.

26 H. An, W. Tian, X. Lu, H. Yuan, L. Yang, H. Zhang, H. Shen and H. Bai, *Chem. Eng. J.*, 2023, **469**, 144052.

27 M. Nazari, F. Zadehahmadi, M. M. Sadiq, A. L. Sutton, H. Mahdavi and M. R. Hill, *Commun. Mater.*, 2024, **5**, 170.

28 W. Morris, S. Wang, D. Cho, E. Auyeung, P. Li, O. K. Farha and C. A. Mirkin, *ACS Appl. Mater. Interfaces*, 2017, **9**, 33413–33418.

29 W. Mao, R. Huang, H. Xu, H. Wang, Y. Huang, S. Huang and J. Zhou, *Polymers*, 2022, **14**(18), 3026.

30 S. Kumari, M. Gusain, B. Y. Lamba and S. Kumar, *J. Mater. Chem. A*, 2025, **13**, 21352–21388.

31 Q. Zhao, H.-M. Hou, G.-L. Zhang, H. Hao, B. Zhu and J. Bi, *Appl. Surf. Sci.*, 2024, **655**, 159639.

32 F. Fang, P. Wang, Z. Zhang, S.-S. Zhang, Y.-Y. Guo, S.-Y. Wang, L. Du and Q.-H. Zhao, *CrystEngComm*, 2024, **26**, 2751–2754.

33 G. V. Demirci, M. T. Baig and A. Kayan, *Int. J. Biol. Macromol.*, 2024, **283**, 137950.

34 S. Edubilli and S. Gumma, *Sep. Purif. Technol.*, 2019, **224**, 85–94.

35 J. H. Cavka, S. Jakobsen, U. Olsbye, N. Guillou, C. Lamberti, S. Bordiga and K. P. Lillerud, *J. Am. Chem. Soc.*, 2008, **130**, 13850–13851.

36 X. Liu, N. K. Demir, Z. Wu and K. Li, *J. Am. Chem. Soc.*, 2015, **137**(22), 6999–7002.

37 M. Taddei, K. C. Dümbgen, J. A. Van Bokhoven and M. Ranocchiari, *Chem. Commun.*, 2016, **52**, 6411–6414.

38 A. A. Abd, M. R. Othman, I. K. Shamsudin, Z. Helwani and I. Idris, *Chem. Eng. J.*, 2023, **453**, 139774.

39 S. Biswas, J. Zhang, Z. Li, Y.-Y. Liu, M. Grzywa, L. Sun, D. Volkmer and P. Van Der Voort, *Dalton Trans.*, 2013, **42**, 4730.

40 R. Grünker, V. Bon, P. Müller, U. Stoeck, S. Krause, U. Mueller, I. Senkovska and S. Kaskel, *Chem. Commun.*, 2014, **50**, 3450.

41 G. E. Decker, Z. Stillman, L. Attia, C. A. Fromen and E. D. Bloch, *Chem. Mater.*, 2019, **31**, 4831–4839.

42 R. D'Amato, R. Bondi, I. Moghdad, F. Marmottini, M. J. McPherson, H. Naïli, M. Taddei and F. Costantino, *Inorg. Chem.*, 2021, **60**, 14294–14301.

43 K. Sladekova, C. Campbell, C. Grant, A. J. Fletcher, J. R. B. Gomes and M. Jorge, *Adsorption*, 2020, **26**, 663–685.

44 M. Taddei, J. A. van Bokhoven and M. Ranocchiari, *Inorg. Chem.*, 2020, **59**, 7860–7868.

45 K. Nikoofar and Z. Khademi, *Res. Chem. Intermed.*, 2016, **42**, 3929–3977.

46 V. Somjit, P. Thinsoongnoen, S. Waiprasoet, T. Pila, P. Pattanasattayavong, S. Horike and K. Kongpatpanich, *ACS Appl. Mater. Interfaces*, 2021, **13**, 30844–30852.

47 K. Tulig and K. S. Walton, *RSC Adv.*, 2014, **4**, 51080–51083.

48 B. Bueken, N. Van Velthoven, T. Willhammar, T. Stassin, I. Stassen, D. A. Keen, G. V. Baron, J. F. M. Denayer, R. Ameloot, S. Bals, D. De Vos and T. D. Bennett, *Chem. Sci.*, 2017, **8**, 3939–3948.

49 N. Chanut, S. Bourrelly, B. Kuchta, C. Serre, J. S. Chang, P. A. Wright and P. L. Llewellyn, *ChemSusChem*, 2017, **10**, 1543–1553.

50 F. Ragon, P. Horcajada, H. Chevreau, Y. K. Hwang, U. H. Lee, S. R. Miller, T. Devic, J. S. Chang and C. Serre, *Inorg. Chem.*, 2014, **53**, 2491–2500.

51 G. C. Shearer, S. Chavan, J. Ethiraj, J. G. Vitillo, S. Svelle, U. Olsbye, C. Lamberti, S. Bordiga and K. P. Lillerud, *Chem. Mater.*, 2014, **26**, 4068–4071.

52 M. Athar, P. Rzepka, D. Thoeny, M. Ranocchiari and J. Anton van Bokhoven, *RSC Adv.*, 2021, **11**, 38849–38855.

53 M. E. DMello, N. G. Sundaram, A. Singh, A. K. Singh and S. B. Kalidindi, *Chem. Commun.*, 2019, **55**, 349–352.

54 Y. Ma, W. Lu, X. Han, Y. Chen, I. da Silva, D. Lee, A. M. Sheveleva, Z. Wang, J. Li, W. Li, M. Fan, S. Xu, F. Tuna, E. J. L. McInnes, Y. Cheng, S. Rudić, P. Manuel, M. D. Frogley, A. J. Ramirez-Cuesta, M. Schröder and S. Yang, *J. Am. Chem. Soc.*, 2022, **144**, 8624–8632.

55 S. Devautour-Vinot, G. Maurin, C. Serre, P. Horcajada, D. Paula da Cunha, V. Guillerm, E. de Souza Costa, F. Taulelle and C. Martineau, *Chem. Mater.*, 2012, **24**, 2168–2177.

56 J. R. Long, B. Q. Sun, A. Bowen and R. G. Griffin, *J. Am. Chem. Soc.*, 1994, **116**, 11950–11956.

57 T. D. Bennett, T. K. Todorova, E. F. Baxter, D. G. Reid, C. Gervais, B. Bueken, B. Van de Voorde, D. De Vos, D. A. Keen and C. Mellot-Draznieks, *Phys. Chem. Chem. Phys.*, 2016, **18**, 2192–2201.

58 C. M. Hangarter, B. Dyatkin, M. Laskoski, M. C. Palenik, J. B. Miller and C. A. Klug, *Appl. Magn. Reson.*, 2022, **53**, 915–930.

59 F. Venel, C. Volkringer, O. Lafon and F. Pourpoint, *Solid State Nucl. Magn. Reson.*, 2022, **120**, 101797.

60 D. Salionov, O. O. Semivrazhskaya, N. P. M. Casati, M. Ranocchiari, S. Bjelić, R. Verel, J. A. van Bokhoven and V. L. Sushkevich, *Nat. Commun.*, 2022, **13**, 3762.

61 D. M. Driscoll, D. Troya, P. M. Usov, A. J. Maynes, A. J. Morris and J. R. Morris, *Phys. Chem. Chem. Phys.*, 2019, **21**, 5078–5085.

62 J. Zhang, M. N. Khan, Z. Hu and J. Zou, *Chem. Commun.*, 2024, **60**, 8395–8398.

63 M. Atsumi, J.-J. Zheng, E. Tellgren, S. Sakaki and T. Helgaker, *Phys. Chem. Chem. Phys.*, 2023, **25**, 28770–28783.

64 Q. Hu, R. Lan, L. He, H. Liu and X. Pei, *J. Environ. Manage.*, 2023, **329**, 117104.

65 R. Essehli, S. Sabri, F. El-Mellouhi, B. Aïssa, H. Ben Yahia, T. Altamash, M. Khraisheh, A. Amhamed and B. El Bali, *Sci. Rep.*, 2020, **10**, 8909.

66 M. He, S. Shi, Z. Liu, Y. Wu and L. Wang, *Chem. Commun.*, 2025, **61**, 5072–5083.

67 Z. Zhu, H. Tsai, S. T. Parker, J.-H. Lee, Y. Yabuuchi, H. Z. H. Jiang, Y. Wang, S. Xiong, A. C. Forse, B. Dinakar, A. Huang, C. Dun, P. J. Milner, A. Smith, P. Guimarães Martins, K. R. Meihaus, J. J. Urban, J. A. Reimer, J. B. Neaton and J. R. Long, *J. Am. Chem. Soc.*, 2024, **146**, 6072–6083.

68 Y. Magnin, E. Dirand, A. Orsikowsky, M. Plainchault, V. Pugnet, P. Cordier and P. L. Llewellyn, *J. Phys. Chem. C*, 2022, **126**, 3211–3220.